



Time dependence of neutrino quantum kinetics in a core-collapse supernova

Shashank Shalgar  ^a and **Irene Tamborra**  ^a

^aNiels Bohr International Academy & DARK, Niels Bohr Institute,
University of Copenhagen, Blegdamsvej 17, 2100 Copenhagen, Denmark

E-mail: shashank.shalgar@nbi.ku.dk, tamborra@nbi.ku.dk

Abstract. Our understanding of neutrino flavor conversion in the supernova core is still preliminary, despite its likely relevance to the neutrino-driven supernova mechanism. We present multi-angle and multi-energy numerical simulations of neutrino quantum kinetics within a spherically symmetric shell in the proximity of the region of neutrino decoupling. We rely on inputs from a one-dimensional core-collapse supernova model with a mass of $18.6 M_{\odot}$ and find that, at early post-bounce times ($t_{pb} \lesssim 0.5$ s), no crossing is present in the angular distribution of the electron neutrino lepton number and flavor conversion develops due to vacuum mixing. Angular crossings appear for $t_{pb} \gtrsim 0.5$ s and fast flavor conversion leads to flavor equipartition, with the spectral energy distribution of ν_e ($\bar{\nu}_e$) and ν_x ($\bar{\nu}_x$) becoming comparable. Notably, flavor equipartition is not a generic outcome of fast flavor conversion, but rather a consequence of the relatively similar properties of neutrinos of different flavors characterizing the late accretion phase. Artificially tweaking the collision term to introduce an electron lepton number angular crossing for $t_{pb} \lesssim 0.05$ s, we observe that flavor equipartition is not achieved. While our findings are restricted to a specific supernova model, they suggest a rich phenomenology of flavor conversion in the supernova core as a function of the post-bounce time which needs to be further explored to assess its impact on the explosion mechanism.

Contents

| | | |
|----------|--|-----------|
| 1 | Introduction | 1 |
| 2 | Neutrino quantum kinetics in spherical symmetry | 2 |
| 2.1 | Quantum kinetic equations | 2 |
| 2.2 | Simulation setup | 4 |
| 3 | Benchmark core-collapse supernova model | 5 |
| 4 | Time dependent neutrino quantum kinetics | 9 |
| 4.1 | Early accretion phase: no ELN crossings, minimal flavor conversion | 9 |
| 4.2 | Late accretion phase: appearance of ELN crossings and fast flavor conversion | 10 |
| 4.3 | Flavor equipartition is not a generic flavor outcome of fast flavor conversion | 12 |
| 5 | Discussion | 12 |
| 6 | Conclusions | 17 |

1 Introduction

In neutrino dense astrophysical sources, flavor evolution is significantly affected by the coherent forward scattering (refraction) of neutrinos with each other [1, 2]. Neutrino self-interaction, however, makes the neutrino equations of motion nonlinear and the consequent flavor evolution displays a rich phenomenology that we are still far from understanding [3–7].

The modification of neutrino flavor evolution due to refraction with other neutrinos can be broadly classified into slow [4, 8, 9], fast [6, 7, 10–14], and collisional [15]. Slow flavor evolution is differentiated from the fast one by the role of the vacuum frequency. In fact, fast flavor evolution can manifest in the limit of vanishing vacuum frequency and it is triggered by a crossing in the electron lepton number (ELN) angular distribution of neutrinos [13, 14, 16], whereas slow flavor evolution requires a nonzero vacuum term [9, 17]. Fast flavor evolution, as the name suggests, occurs over very small time scales—the characteristic frequency being directly proportional to the number density of neutrinos. On the other hand, collisional instabilities should be triggered by neutrino collisions with the medium in the high-density region in the proximity of neutrino decoupling [18–21], but their relevance on flavor conversion physics within realistic astrophysical environments remains to be assessed [22, 23].

Neutrinos play a crucial role in the core-collapse supernova mechanism [24, 25], as recently confirmed by multi-dimensional hydrodynamic simulations [26–29]. Whether neutrino flavor conversion, triggered by any of the flavor instabilities highlighted above, affects the core collapse mechanism is the subject of ongoing research [30–32]. Preliminary work suggests that, if flavor equilibration should occur as a result of such instabilities, this would facilitate or hinder the supernova explosion according to the mass of the collapsing star [31]. Because of the technical challenges linked to the solution of the neutrino quantum kinetic equations (QKEs) and the vast difference in the characteristic scales typical of the source hydrodynamics and the ones entering the neutrino equations of motion, a self-consistent solution of this problem is not yet available [6, 7]. Nevertheless, it is possible to search for general trends by

solving the QKEs within a simulation shell, taking into account the interplay among flavor evolution, collisions, and advection. In this case, a quasi-steady state configuration is found in the aftermath of flavor conversion [22, 32–38].

An open question concerns whether flavor equipartition is a general solution of the QKEs. While recent work seems to point in this direction [36, 39–49], the boundary conditions as well as the ELN distribution entering the solution of the QKEs could drastically affect the final flavor configuration [33, 34, 37]. In this paper, we investigate the neutrino flavor evolution in spherical symmetry, relying on input from several post-bounce time snapshots within 1 s of a one-dimensional hydrodynamic simulation of a core-collapse supernova with a mass of $18.6 M_{\odot}$ [50]. We find that, in the early accretion phase ($t_{\text{pb}} \lesssim 0.5$ s), flavor conversion is driven by vacuum mixing; while, in the late accretion phase ($t_{\text{pb}} \gtrsim 0.5$ s), equipartition between the neutrino spectral energy distributions of ν_e and ν_x as well as $\bar{\nu}_e$ and $\bar{\nu}_x$. Yet, we confirm early findings [33, 34, 37] showing that flavor equipartition is not a general flavor outcome for any given unstable flavor configuration.

This paper is organized as follows. Section 2 introduces the neutrino QKEs and outlines the approach adopted to model the collision term as well as the simulation setup. In Sec. 3, we describe the main features of our benchmark one-dimensional supernova model, compute the neutrino angular distributions of all flavors employing a multi-energy transport scheme and illustrate as they evolve as functions of the post-bounce time. Our main findings are presented in Sec. 4. Finally, we discuss our results in Sec. 5 and conclude in Sec. 6.

2 Neutrino quantum kinetics in spherical symmetry

In this section, we introduce the neutrino equations of motion. We also outline the numerical techniques adopted to solve the neutrino QKEs.

2.1 Quantum kinetic equations

For simplicity, we consider two neutrino flavors (ν_e and ν_x with $x = \mu, \tau$), and the corresponding antineutrinos ($\bar{\nu}_e$ and $\bar{\nu}_x$). We model our neutrino ensemble in terms of 2×2 density matrices for neutrinos and antineutrinos for each radial location (r), polar angle (θ), and energy (E), as a function of time (t) and under the assumption of spherical symmetry, see Fig. 1¹. The diagonal elements of the density matrices (ρ_{ii} with $i = e$ and x) represent the neutrino occupation number and are normalized such $\int_{-1}^1 \rho(r, \cos \theta, E, t) dE d \cos \theta$ gives the local neutrino number density of flavor i at a given radius (n_{ν_i}).

The equations of motion that describe the evolution of the (anti)neutrino density matrices are:

$$i \left(\frac{\partial}{\partial t} + \vec{v} \cdot \vec{\nabla} \right) \rho(r, \cos \theta, E, t) = [H(r, \cos \theta, E, t), \rho(r, \cos \theta, E, t)] + i\mathcal{C}[\rho], \quad (2.1)$$

$$i \left(\frac{\partial}{\partial t} + \vec{v} \cdot \vec{\nabla} \right) \bar{\rho}(r, \cos \theta, E, t) = [\bar{H}(r, \cos \theta, E, t), \bar{\rho}(r, \cos \theta, E, t)] + i\bar{\mathcal{C}}[\bar{\rho}]. \quad (2.2)$$

The total derivative on the left hand side of Eqs. 2.1 and 2.2 consists of a partial derivative with respect to time and the advective term, which is in spherical symmetry

$$\vec{v} \cdot \vec{\nabla} = \cos \theta \frac{\partial}{\partial r} + \frac{\sin^2 \theta}{r} \frac{\partial}{\partial \cos \theta}. \quad (2.3)$$

¹Note that the polar angle θ is defined with respect to the radial direction at a given point and it is not the emission angle used in the early papers on neutrino-bulb model [4, 8, 9].

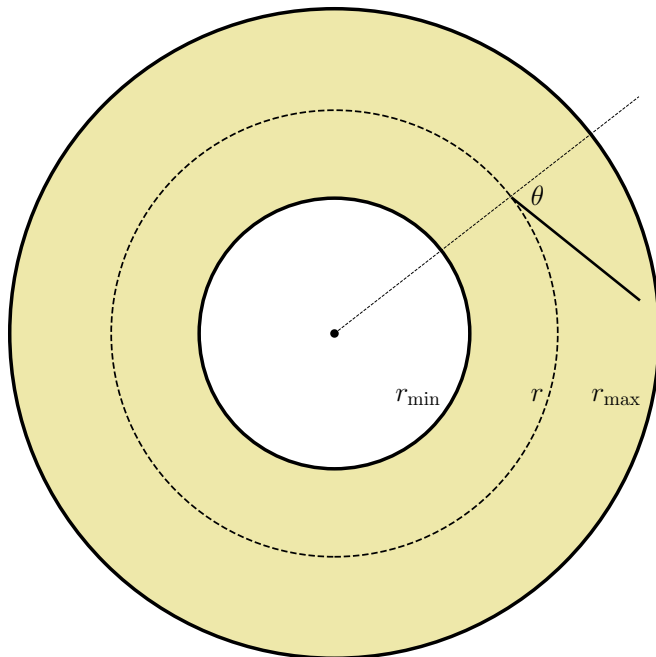


Figure 1. Sketch of the simulation shell adopted to solve the QKEs. The polar angle θ is defined with respect to the radial direction and it is a function of radius (r) for any given trajectory. The radii r_{\min} and r_{\max} denote the innermost and outermost radii adopted in the simulation.

The advective term is such that, in the absence of any term other than the total derivative, neutrinos travel along a straight line. General relativistic effects are neglected in Eqs. 2.1 and 2.2, qualitatively they should not affect the interplay between neutrino flavor conversion and transport effects on small scales [32].

On the right hand side of Eqs. 2.1 and 2.2, the commutator of the Hamiltonian and the density matrix takes into account neutrino flavor conversion physics. The Hamiltonian consists of three components: the vacuum, matter, and self-interaction terms. The matter term effectively suppresses the mixing angle in the vacuum term; hence, we choose to adopt an effective vacuum mixing angle, ignoring the matter term:

$$H(r, \cos \theta, E, t) = H_{\text{vac}}(E) + H_{\nu\nu}(r, \cos \theta, t) \text{ and } \bar{H}(r, \cos \theta, E, t) = -H_{\text{vac}}(E) + H_{\nu\nu}(r, \cos \theta, t). \quad (2.4)$$

The vacuum and self-interaction terms are defined as

$$H_{\text{vac}}(E) = \frac{\omega_{\text{vac}}}{2} \begin{pmatrix} -\cos 2\vartheta_V & \sin 2\vartheta_V \\ \sin 2\vartheta_V & \cos 2\vartheta_V \end{pmatrix}, \quad (2.5)$$

$$H_{\nu\nu}(r, \cos \theta, t) = \sqrt{2}G_{\text{F}}\xi \int_{-1}^1 [\rho(r, \cos \theta', E, t) - \bar{\rho}(r, \cos \theta', E, t)] \times (1 - \cos \theta \cos \theta') dE d \cos \theta'. \quad (2.6)$$

The vacuum frequency is $\omega_{\text{vac}} = \Delta m^2/2E$ with $\Delta m^2 = 2.5 \times 10^{-3} \text{ eV}^2$, and $\vartheta_V = 10^{-3} \text{ rad}$ denotes the matter suppressed mixing angle. The self-interaction Hamiltonian, unlike the vacuum Hamiltonian, depends on θ and is obtained integrating over all momentum modes.

The integration over the azimuthal angle results in a constant factor 2π that has been absorbed in the definition of the density matrices. On the other hand, the self-interaction Hamiltonian does not depend on energy. Following the attenuation method introduced in Ref. [51], we rescale the strength of neutrino self-interaction by a constant factor $\zeta = 10^{-3}$. The choice of ζ is such that the self-interaction strength is always larger than ω at neutrino decoupling and the quasi-steady state flavor state configuration is likely not affected, but the time needed for reaching such a configuration changes with the computational time being reduced [52, 53].

The collision term on the right hand side of Eqs. 2.1 and 2.2, represented by \mathcal{C} and $\bar{\mathcal{C}}$, includes three contributions: the emission term ($\mathcal{C}^{\text{emit}}$), the absorption term ($\mathcal{C}^{\text{absorb}}$), and the direction changing term ($\mathcal{C}^{\text{dir-ch}}$) [28, 54, 55]. For all flavors of neutrinos, pair production and Bremsstrahlung contribute to the emission and absorption terms, whereas the beta processes only contribute to electron-type neutrinos and antineutrinos. The direction changing term is given by the neutral current interaction between neutrinos and nucleons, which are assumed to be elastic. The inelastic contribution is negligible for the electron type neutrinos and thus does not affect the presence of ELN crossings. The collision terms are defined as follows:

$$\begin{aligned} \mathcal{C}[\rho] = & \mathcal{C}^{\text{emit}}(r, E) - \mathcal{C}^{\text{absorb}}(r, E) \odot \rho(r, \cos \theta, E) + \cos \theta \mathcal{C}_{\text{ani}}(r, E) \int d \cos \theta' \cos \theta' \rho(r, \cos \theta', E) \\ & + \frac{\mathcal{C}^{\text{dir-ch}}(r, E)}{2} \int d \cos \theta' [-\rho(r, \cos \theta, E) + \rho(r, \cos \theta', E)] ; \end{aligned} \quad (2.7)$$

we use the symbol \odot to denote the elementwise multiplication:

$$\mathcal{C}_{\text{absorb}}(E) \odot \rho(\cos \theta, E) = \begin{pmatrix} \mathcal{C}_{\text{absorb}}^{ee}(E) \rho_{ee}(\cos \theta, E) & \mathcal{C}_{\text{absorb}}^{ex}(E) \rho_{ex}(\cos \theta, E) \\ \mathcal{C}_{\text{absorb}}^{xe}(E) \rho_{xe}(\cos \theta, E) & \mathcal{C}_{\text{absorb}}^{xx}(E) \rho_{xx}(\cos \theta, E) \end{pmatrix} . \quad (2.8)$$

The emission and absorption terms are related by Kirchoff's law for each energy, $\mathcal{C}^{\text{emit}}(E)/\mathcal{C}_{\text{absorb}}(E) = f_{\text{FD}}(E)$, where $f_{\text{FD}}^{\nu_i}(E) = dn_{\nu_i}/dE$ is the Fermi-Dirac energy distribution. An analogous expression holds for $\mathcal{C}[\bar{\rho}]$. The terms \mathcal{C}_{ani} and $\bar{\mathcal{C}}_{\text{ani}}$ are included out of completeness and take into account the anisotropic nature of direction changing neutral current interactions. The collision terms used in this paper are the multi-energy extension of the ones presented in Appendix A of Ref. [23], which in turn are based on Refs. [56, 57].

2.2 Simulation setup

In order to solve the QKEs, we use the Julia implementation of the Adam-Moulton multi-step integrator, with adaptive order and adaptive step size for the time variable ² (VCABM solver). The spatial derivatives in the advective term are calculated using the central difference method. To discretize the density matrix, we employ 75 angle bins, 24 energy bins for $E \in [0, 50]$ MeV, and 150 radial bins for $r \in [r_{\text{min}}, r_{\text{max}}]$ (with r_{min} and r_{max} being the innermost and outermost radii of our simulation shell; see Fig. 1).

Our goal is to compute the ‘‘quasi-steady state’’ configuration achieved by the system ³. The latter should be independent of the initial configuration, but the choice of the initial

²The length scale characteristic of our neutrino ensemble is not given by the inverse of the self-interaction potential, rather it is a combination of the collision term and the self-interaction potential [33, 34]. Yet, it is important to ensure that the time step is much smaller than the inverse of the neutrino self-interaction strength; we do this by implementing an adaptive step size.

³A quasi-steady state configuration does not coincide with the solution of the boundary value problem obtained by setting the time derivative to zero. The quasi-steady state is also not approximately close to the

Table 1. Values of r_{\min} and r_{\max} chosen for each post-bounce time snapshot in order to capture the radial region of neutrino decoupling (see also Fig. 1).

| t_{pb} (s) | r_{\min} (km) | r_{\max} (km) |
|---------------------|-----------------|-----------------|
| 0.05 | 25 | 150 |
| 0.12 | 25 | 100 |
| 0.25 | 22 | 57 |
| 0.5 | 20 | 35 |
| 0.75 | 17 | 32 |
| 1 | 16 | 31 |

configuration does affect the efficiency and numerical stability of the numerical solution. As pointed out in Refs. [33, 34], the most efficient way to tackle this issue numerically is to first solve Eqs. 2.1 and 2.2 for $H = \bar{H} = 0$ to obtain the “classical steady state” solution (i.e., we solve the classical Boltzmann equation). We then use the classical steady state solution as the initial configuration to solve Eqs. 2.1 and 2.2 for $H \neq 0$ and $\bar{H} \neq 0$. This approach has two advantages. First, it is easier to highlight the impact of flavor evolution; second, the initial classical steady state configuration is not too different from the final quasi-steady state. We stress, however, that the choice to use the classical solution as the initial configuration is not unique, in principle it might be possible to devise a better initial configuration.

For obtaining the classical steady-state solution as well as the quasi-steady state one, the radial range has to be chosen such that the neutrino spectral energy distributions coincide with Fermi-Dirac distributions at the minimum radius (r_{\min}); whereas the maximum radius (r_{\max}) is chosen such that the classical solution has negligible backward flux [23], see also Fig. 1 and Table 2.2. These conditions serve as boundary conditions for Eqs. 2.1 and 2.2. The hydrodynamic and thermodynamic supernova properties employed to compute the classical and quasi-steady state configurations are extracted from a one-dimensional core-collapse supernova simulation whose features are illustrated in Sec. 3.

3 Benchmark core-collapse supernova model

We rely on the outputs of a one-dimensional hydrodynamic simulation of a $18.6 M_{\odot}$ core-collapse supernova, with $1.4 M_{\odot}$ gravitational mass and SFHo nuclear equation of state without muons [50]. In this model, the effects of proto-neutron star convection have been taken into account through a mixing-length approximation [3, 58].

We focus on few selected post-bounce times ($t_{\text{pb}} = 0.05, 0.12, 0.25, 0.5, 0.75, \text{ and } 1 \text{ s}$) and rely on static hydrodynamic backgrounds and thermodynamical quantities for each time snapshot to compute the classical steady-state neutrino configuration. Figure 2 shows the radial evolution of the main supernova properties entering the collision term in Eqs 2.1 and 2.2.

Since the neutrino angular distributions are not provided as an output of our benchmark hydrodynamic simulation, we compute them following the same procedure illustrated in Sec. III of Ref. [23], i.e. we set r_{\min} and r_{\max} as indicated in Table 2.2 for each snapshot

solution of that boundary value problem. The reason for this counter-intuitive assertion is that, if Eqs. 2.1 and 2.2 are evolved for a long enough time, ρ_{ee} , ρ_{xx} and $|\rho_{ex}|$ reach a steady state, but the phase of ρ_{ex} does not converge towards a steady state. This explains why we need to evolve the system as a function of time instead of attempting to find a solution to Eqs. 2.1 and 2.2 setting the time derivative to zero.

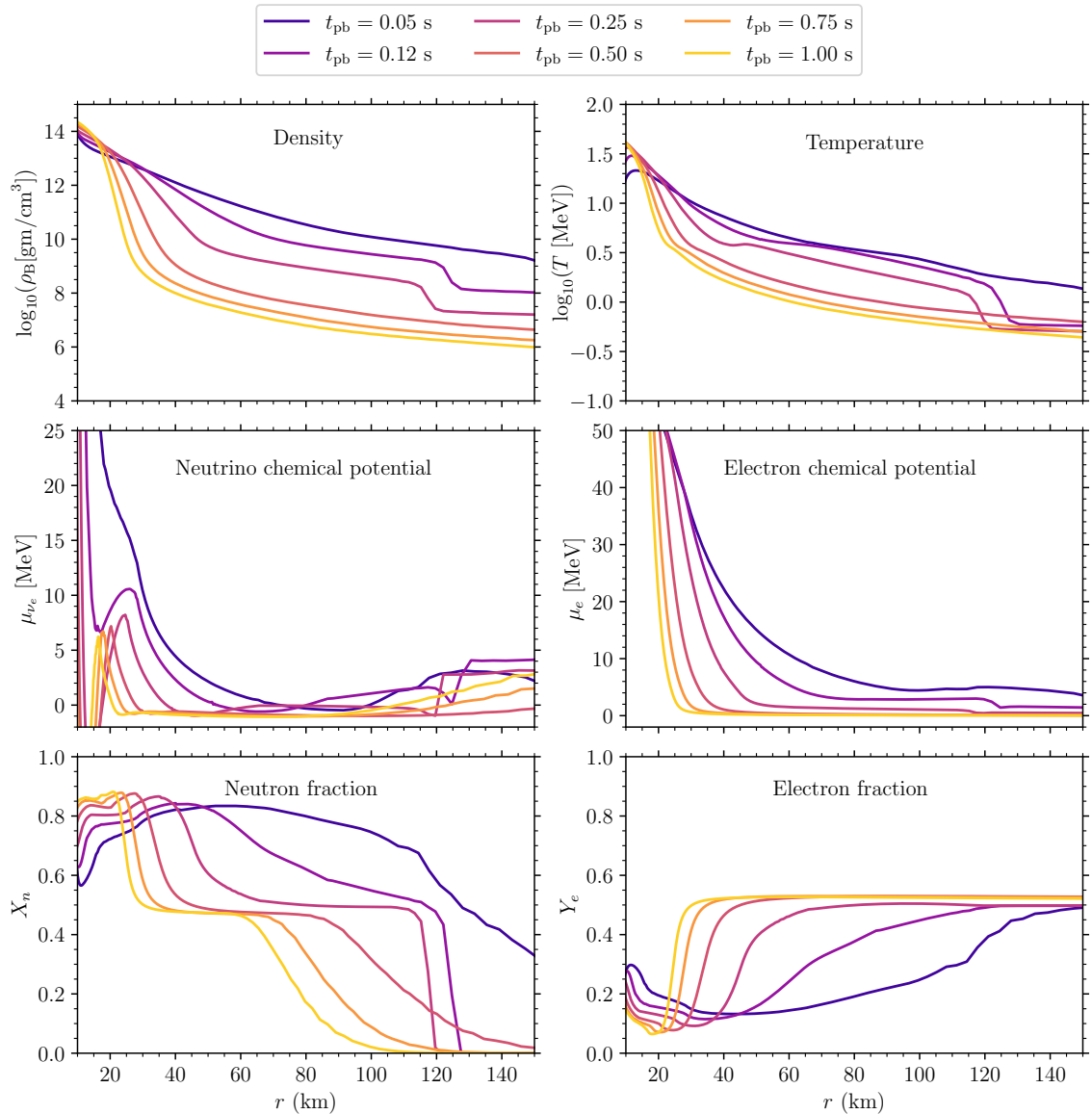


Figure 2. Radial profiles of the characteristic quantities extracted from our core-collapse supernova model (see main text for details) at $t_{\text{pb}} = 0.05, 0.12, 0.25, 0.5, 0.75,$ and 1 s. From top left to bottom right, each panel represents the radial evolution of the baryon number density, the electron temperature, the neutrino and electron chemical potentials, and the neutron and electron fractions, respectively.

and solve Eqs. 2.1 and 2.2 for $H = \bar{H} = 0$. In contrast to Ref. [23], we compute the angular distributions of (anti)neutrinos solving Eqs. 2.1 and 2.2 for multiple energy modes (see Sec. 2.2).

The left panels of Figs. 3 and 4 display the contour plot of the energy-integrated $\rho_{ee} - \bar{\rho}_{ee}$ in the plane spanned by $\cos\theta$ and r in the absence of flavor conversion (i.e., the classical steady state configuration). One can see that, at small radii (before neutrino decoupling), the angular distributions of neutrinos and antineutrinos are isotropic with an overall excess of ν_e . At larger radii, (anti)neutrinos start to decouple from matter entering the free streaming

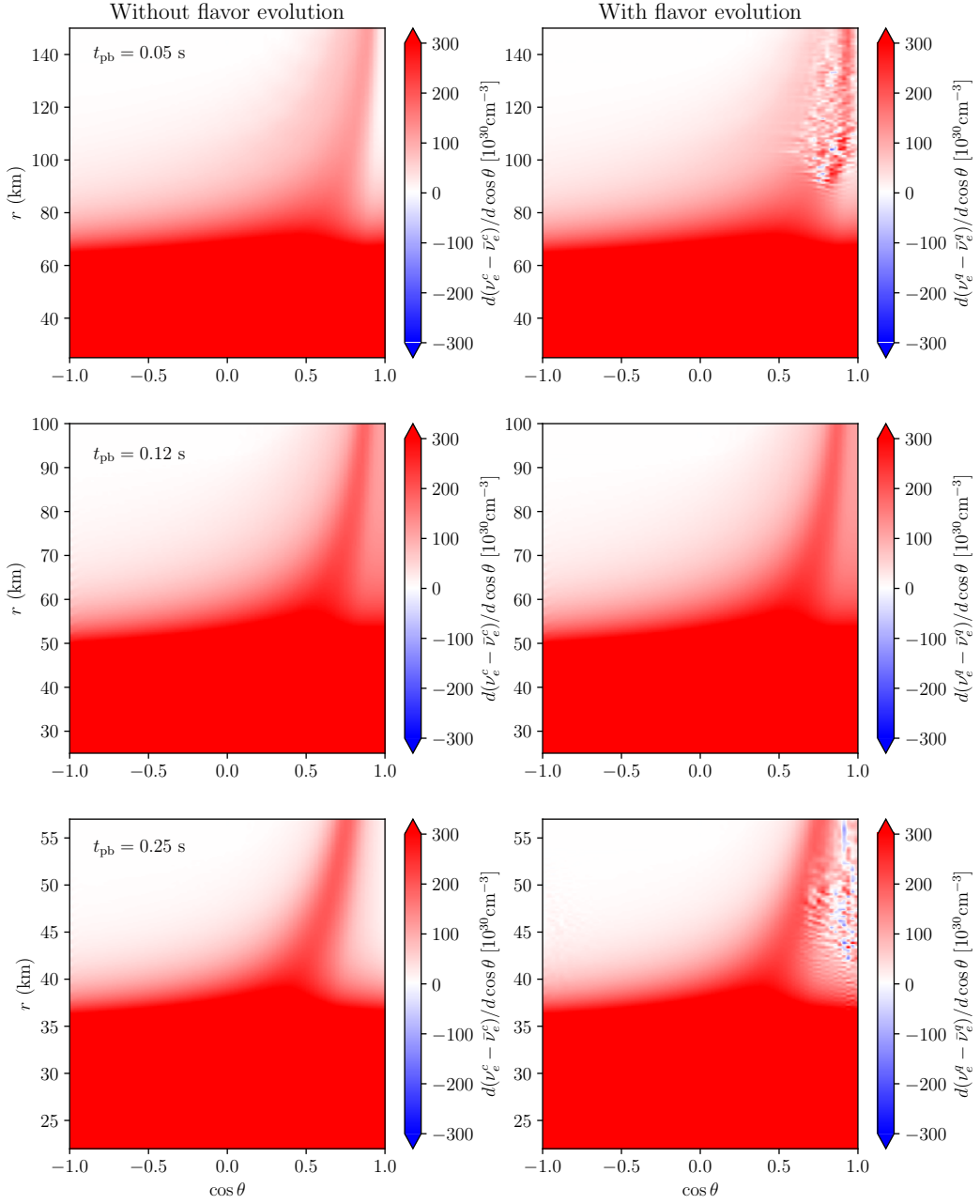


Figure 3. *Left:* Contour plots of the energy-integrated ELN without flavor conversion ($\rho_{ee} - \bar{\rho}_{ee}$, classical solution) for $t_{\text{pb}} = 0.05, 0.12,$ and 0.25 s, from top to bottom respectively. At small radii, the neutrino angular distributions of all flavors are isotropic. In the proximity of neutrino decoupling, the angular distributions start becoming forward peaked, but no ELN crossing develops. The white shade in the top-left corners corresponds to a region with no neutrinos. *Right:* Same as the left column, but with neutrino flavor conversion included ($\rho_{ee} - \bar{\rho}_{ee}$, quantum solution); the QKEs have been evolved for $t = 1.25 \times 10^{-4}$ s. For $t_{\text{pb}} = 0.12$ s, no flavor evolution is seen, but for $t_{\text{pb}} = 0.05$ and 0.25 s flavor evolution occurs due to vacuum mixing, despite the absence of ELN crossings.

regime. As expected, because of the overall decrease of baryon density, neutrinos decouple at smaller radii as the post-bounce time increases. As (anti)neutrinos approach the free-

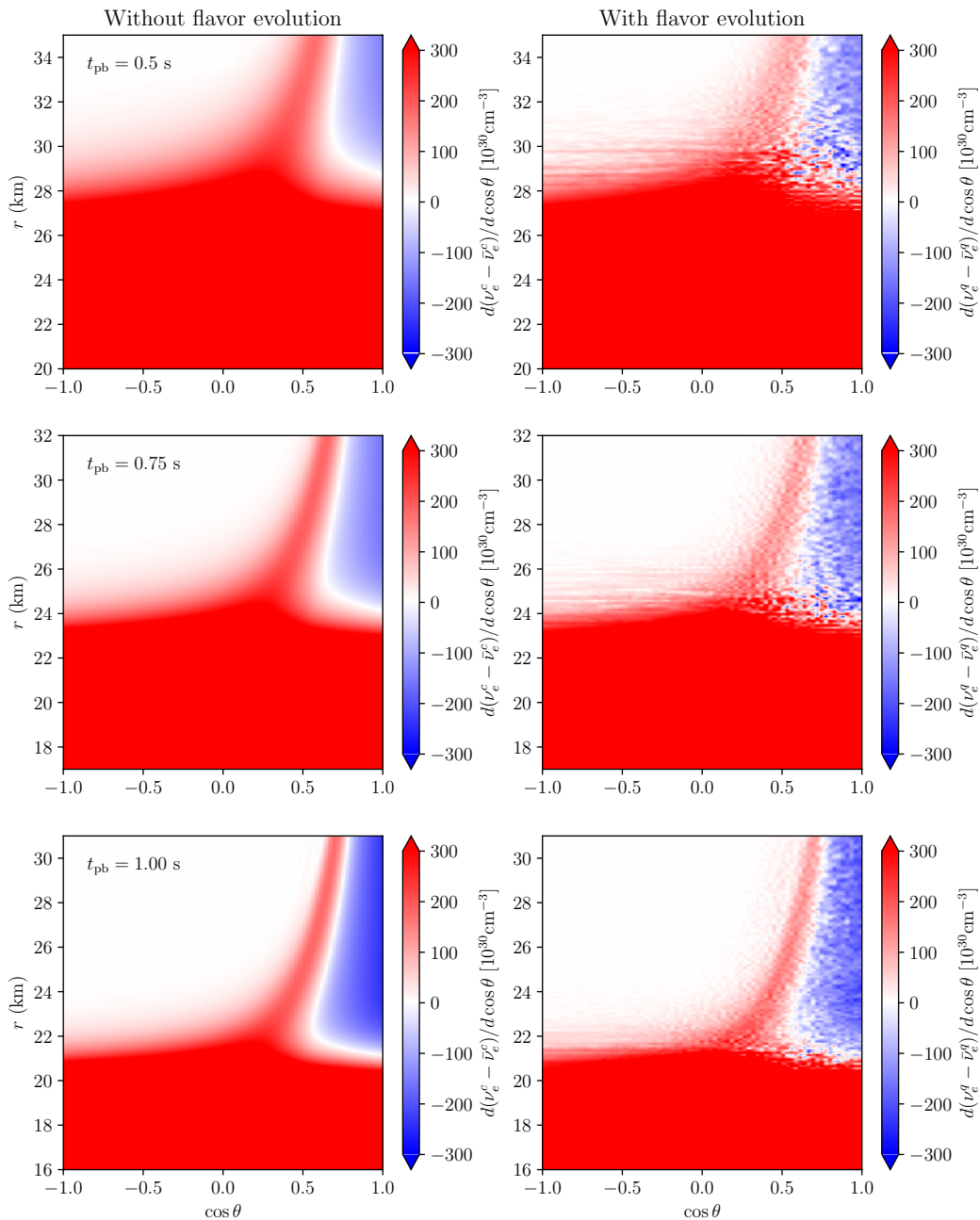


Figure 4. Same as Fig. 3 but for $t_{\text{pb}} = 0.5, 0.75,$ and 1 s, from top to bottom respectively. In the proximity of neutrino decoupling, the angular distributions start becoming forward peaked and ELN crossings develop. The latter are marked by the white contour separating the red and blue regions. In the proximity of ELN crossings, fast flavor conversion develops as expected (the QKEs have been evolved for $t = 7.5 \times 10^{-5}$ s).

streaming regime, an ELN crossing forms for $t_{\text{pb}} \gtrsim 0.5$ s (visible from the white contour separating the red from the blue regions in the left panels of Fig. 4). The presence of an ELN crossing is a necessary condition for flavor instability and becomes a sufficient condition, if periodic boundary conditions are assumed [14, 59].

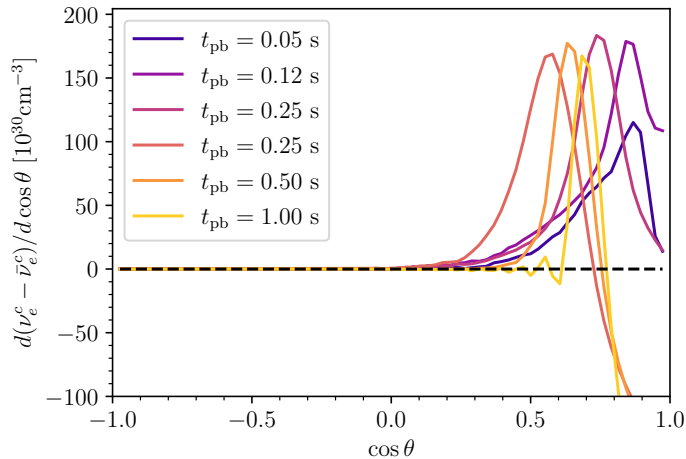


Figure 5. Energy integrated ELN distributions as functions of $\cos\theta$ for our selected post-bounce time snapshots. An ELN crossing appears for $t_{\text{pb}} \gtrsim 0.5$ s; the horizontal black dashed line marks ELN = 0.

Figure 5 shows the energy-integrated ELN angular distributions, extracted at r_{max} , as functions of $\cos\theta$ for our selection of post-bounce time snapshots. We can see that ELN crossings appear for $t_{\text{pb}} \gtrsim 0.5$ s and are not present at early times. However, there is no monotonic trend as a function of radius for what concerns the ELN appearance at different t_{pb} . It is worth noticing that Ref. [23] found ELN crossings for all considered post-bounce time snapshots because it considered a single-energy solution of Eqs. 2.1 and 2.2 for the sake of simplicity. We use this set of classical steady state configurations to investigate the differences in the flavor conversion outcome, as illustrated in the next section.

4 Time dependent neutrino quantum kinetics

In this section, we present our results on the solution of the QKEs for different supernova time snapshots. First, we focus on the early accretion phase ($t_{\text{pb}} \lesssim 0.5$ s) and then we investigate the quasi-steady state configuration during the late accretion phase ($t_{\text{pb}} \gtrsim 0.5$ s). Finally, we artificially modify the collision term to investigate whether flavor equipartition is a generic outcome of flavor conversion.

4.1 Early accretion phase: no ELN crossings, minimal flavor conversion

Although we do not find ELN crossings at early times ($t_{\text{pb}} \lesssim 0.5$ s), this does not imply the absence of flavor evolution as displayed in the right panels of Fig. 3 for $t_{\text{pb}} = 0.05$ and 0.25 s. Such flavor evolution is triggered by the vacuum mass term. Earlier work concluded that slow flavor evolution should be suppressed at early post-bounce times due to the large ratio of the self-interaction strength and the vacuum term [60–65]. However, as recently shown in Ref. [66], if the ELN distribution is on the verge of developing a crossing, the vacuum term can induce a flavor instability even when the self-interaction strength is large (inducing a crossing in the effective ELN distribution). This is exactly what happens at $t_{\text{pb}} = 0.05$ and 0.25 s. We verify this conjecture by performing the linear stability analysis without rescaling the self-interaction strength. As shown in Fig. 6, a non-zero growth rate k of the off-diagonal term of the density matrix is found.

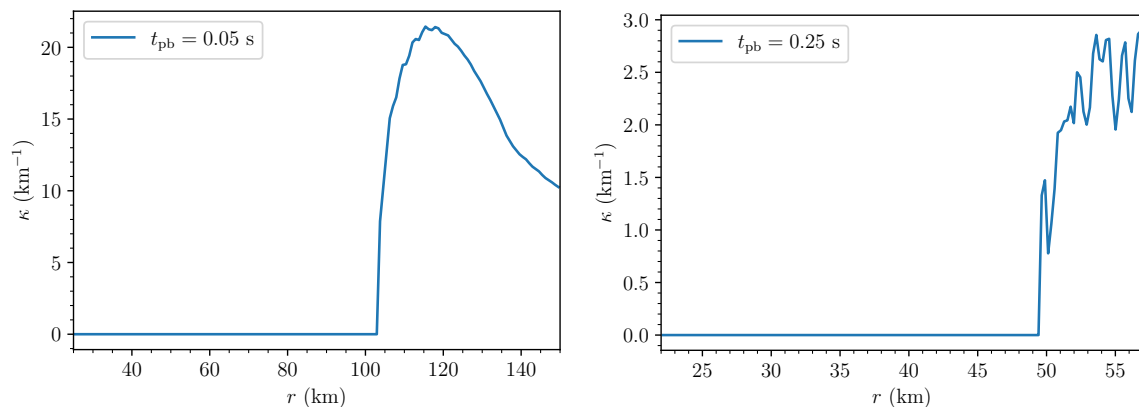


Figure 6. *Left:* Growth rate of the off-diagonal term of the density matrix for $t_{\text{pb}} = 0.05$ s without rescaling of the self-interaction strength and adopting the average energy of the spectral energy distributions of ν_e and $\bar{\nu}_e$. The nonzero growth rate highlights the presence of a flavor instability, despite the absence of an ELN crossing (cf. left panels of Fig. 3). *Right:* Same as the left, but for $t_{\text{pb}} = 0.25$ s. The growth rate is much smaller than that for $t_{\text{pb}} = 0.05$ s, but it is non-zero.

The right panels of Fig. 3 show that, unlike for the flavor instability induced by an ELN crossing (see Sec. 4.2), flavor equipartition does not take place. This can be attributed to a growth rate that does not dominate over the advective length scale as in the case of fast flavor instability and the different shape of the ELN angular distribution (which exhibits a larger difference between the properties of ν_e and $\bar{\nu}_e$ with respect to later post-bounce times).

4.2 Late accretion phase: appearance of ELN crossings and fast flavor conversion

The right panels of Fig. 4 show the contour plots of the energy-integrated $\rho_{ee} - \bar{\rho}_{ee}$ at the simulation time $t = 7.5 \times 10^{-5}$ s in the plane spanned by $\cos\theta$ and r and in the presence of flavor conversion for $t_{\text{pb}} = 0.5, 0.75$ and 1 s (from top to bottom respectively). We find that flavor conversion develops in the proximity of the ELN crossings (the latter being denoted by the white region in between the red and blue ones) for $t_{\text{pb}} = 0.5, 0.75$ and 1 s. Flavor conversion is therefore driven by fast flavor instabilities, as expected from the preliminary findings of Ref. [23] in the single-energy approximation. In fact, Ref. [23] found that the growth rate of the fast flavor instability is four orders of magnitude larger than the collisional instability one for these time snapshots (cf. their Fig. 6). Reference [23] also found that collisional instabilities are present within small spatial regions at smaller radii, yet we do not see any significant flavor conversion linked to them.

In order to investigate whether flavor equipartition is achieved as a result of flavor conversion, Fig. 7 displays the energy-integrated $\rho_{ee} - \rho_{xx}$ for the quasi-steady-state solution obtained after flavor conversion for neutrinos (antineutrinos) on the left (right) panels. Note that, in the region of neutrino trapping, there is an excess of ν_e over ν_x due to the positive chemical potential of ν_e ; while the opposite is true for antineutrinos. For all analyzed configurations for $t_{\text{pb}} \gtrsim 0.5$ s, we find flavor equipartition is achieved for neutrinos and antineutrinos. This is also visible from the left panels of Fig. 9, where the radial evolution of the neutrino number density of the different flavors after flavor conversion (quantum solution) is compared to the one obtained neglecting flavor conversion (classical solution). In particular,

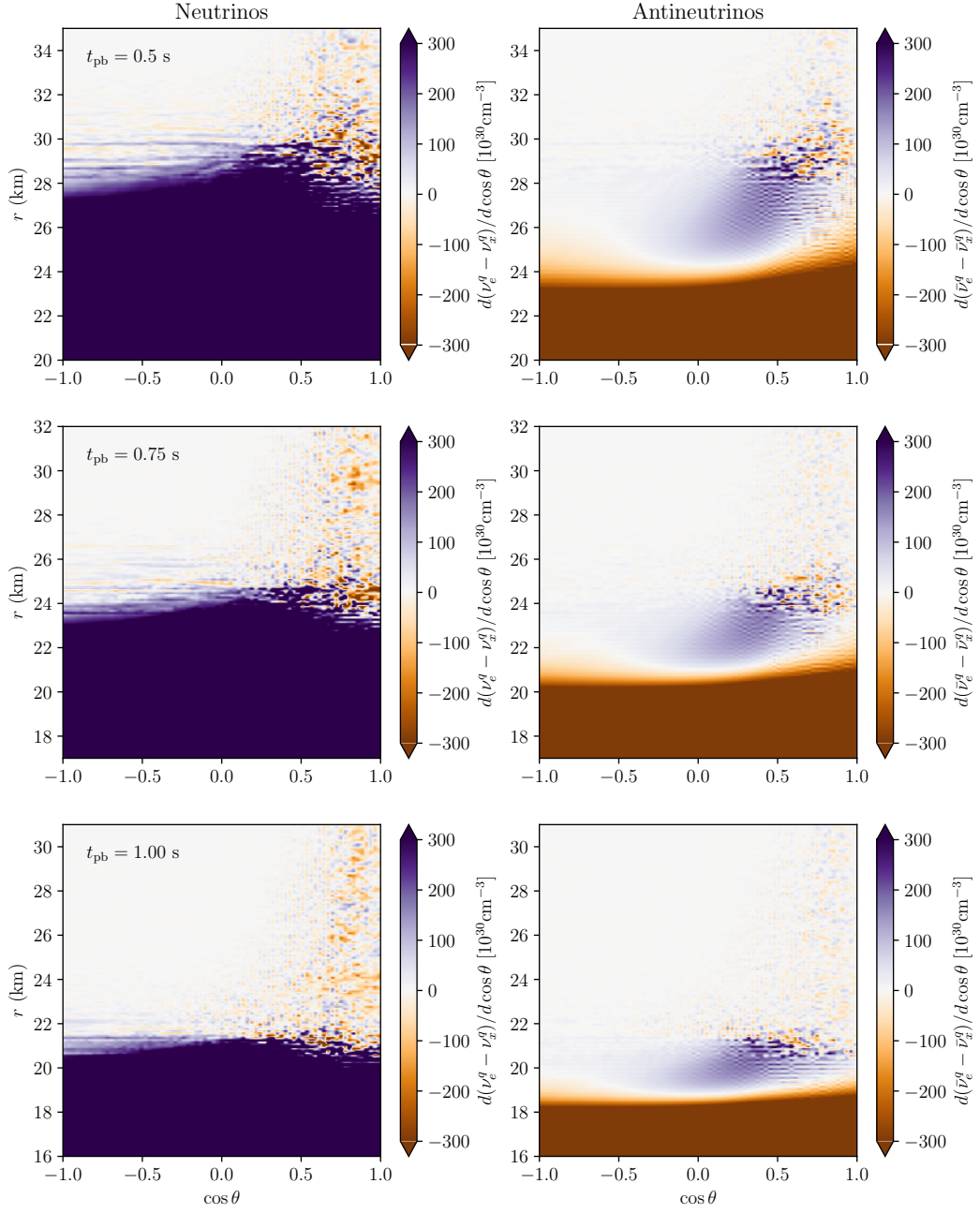


Figure 7. *Left:* Contour plots of the energy-integrated quasi-steady state configuration of $\rho_{ee} - \rho_{xx}$ (quantum solution) for $t_{pb} = 0.5, 0.75,$ and 1 s, from top to bottom respectively (the simulation has been evolved for $t = 7.5 \times 10^{-5}$ s). *Right:* Same as the left column but for antineutrinos. As a result of flavor conversion, flavor equipartition is achieved at large radii, after neutrino decoupling, for neutrinos and antineutrinos ($\rho_{ee} \simeq \rho_{xx}$ and $\bar{\rho}_{ee} \simeq \bar{\rho}_{xx}$; see also Fig. 9).

as shown in the right panels of Fig. 9 for $t_{pb} = 0.5$ (top two panels) and 1 s (bottom two panels), the angle-integrated energy distribution of ν_e ($\bar{\nu}_e$) is identical to the one of ν_x ($\bar{\nu}_x$) in the quasi-steady state configuration and at large radii (r_{\max} has been chosen to extract the spectral distributions plotted in Fig. 9, although any radius after neutrino decoupling shows

a similar trend).

In the left panels of Fig. 9, the decoupling radii for each neutrino flavor are marked by vertical lines. The decoupling radius has been computed as the radius at which the flux factor is equal to 1/3 [33, 67, 68]. We can see that the decoupling radius is minimally affected by flavor conversion (cf. dashed vs. solid lines); in fact, as shown in Ref. [33], the impact of flavor conversion on the decoupling physics strongly depends on the initial ELN distribution and how similar the electron and non-electron flavor emission properties are in the absence of flavor conversion.

4.3 Flavor equipartition is not a generic flavor outcome of fast flavor conversion

The neutrino properties obtained in the late accretion phase tend to be similar to each other for the different post-bounce times that we have considered (cf. Figs. 3, 4 and 9). In order to assess whether flavor equipartition should be expected to be the general flavor outcome of any quasi-steady state configuration, we increase the emission term of $\bar{\nu}_e$ at $t_{\text{pb}} = 0.05$ s by 20% to induce an ELN crossing. Solving the QKEs numerically, we find that flavor equipartition is not reached in the quasi-steady state solution, as shown in Fig. 10.

This flavor outcome can be explained by looking at the number density of ν_e and $\bar{\nu}_e$ in the region of flavor instability: the two differ substantially compared to the configurations obtained at later post-bounce times for which flavor equipartition was found. The observed quasi-steady state configuration is due to the fact that the collision term tends to enhance the ν_e number density and suppress the ν_x one. On the other hand, flavor conversion tends to push ν_e and ν_x towards each other. As a result, the ν_x number density tends to change more (moving upwards) in the quasi-steady state configuration than the ν_e one with respect to the classical solution, being the impact of the collision term smaller for the non-electron flavors. As a consequence, the decoupling radii are also more largely affected by flavor conversion than observed for the other flavor configurations (cf. Fig. 4).

Figure 11 shows the spectral energy distributions extracted for 200 selected time steps at $r = 125$ km and 150 km, in order to investigate the temporal evolution of the quasi-steady flavor configuration. The neutrino spectra continue to oscillate in time, changing by as much as 10%. However, the system is approximately in partial equipartition for the neutrino sector and not for the antineutrino sector at $r = 125$ km (cf. left panel). This trend changes as a function of radius, e.g. the opposite is true for $r = 150$ km (cf. right panel), and in general clearly shows that flavor equipartition is not achieved for this flavor configuration.

We note that the time over which flavor evolution occurs is much shorter than the time scale over which the collision term changes. The continued temporal evolution of the spectral energy distributions suggests that the physically relevant quantities with potential feedback on the source physics should be the average of the bands in Fig. 11.

5 Discussion

In order to assess the possible impact of our findings on neutrino flavor conversion physics on the supernova mechanism, Fig. 12 shows the ratio of the neutrino heating rates obtained relying on the quasi-steady state configuration when the QKEs are solved with and without the commutator term encapsulating the flavor conversion physics. The heating rate is defined

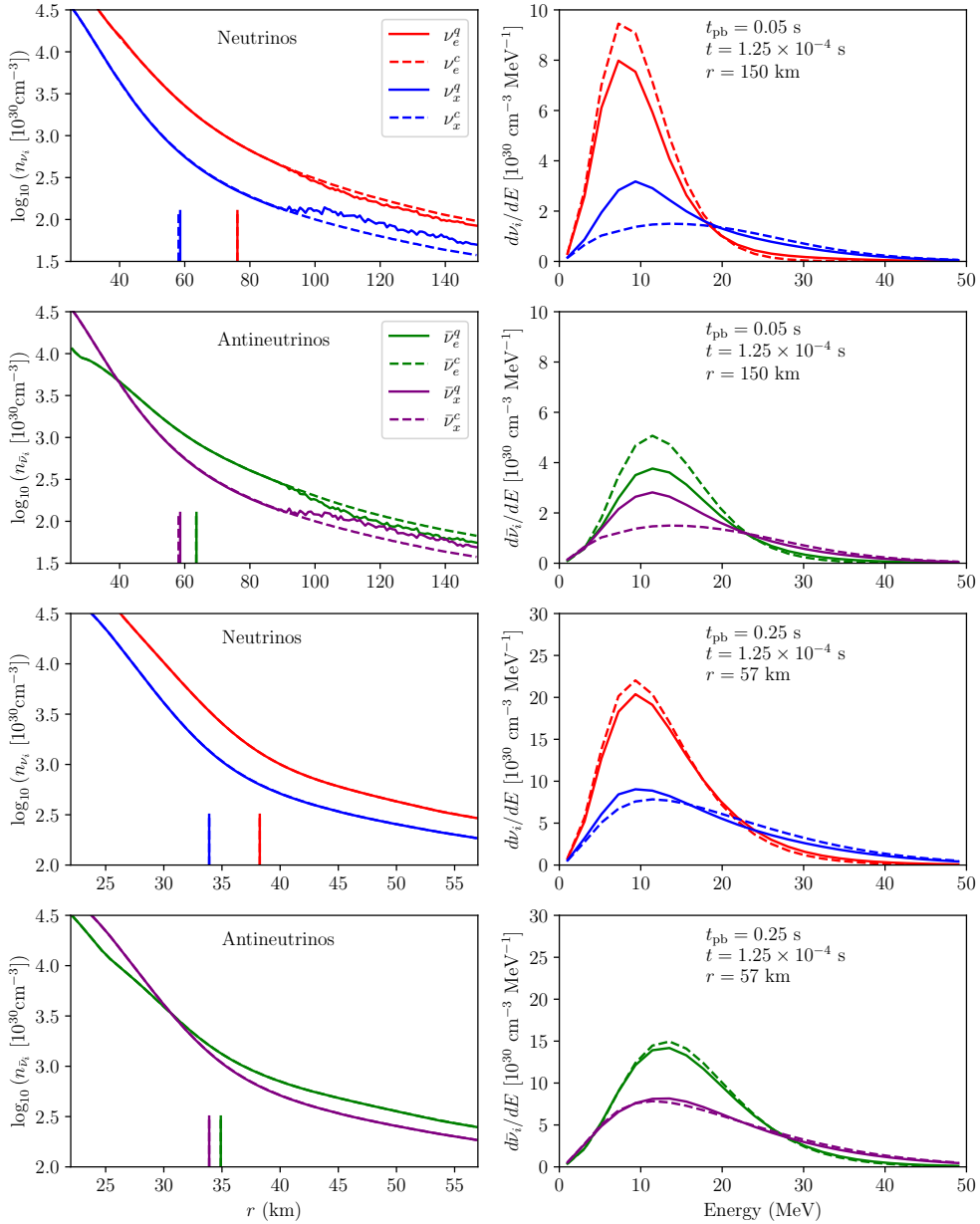


Figure 8. *Left:* Angle and energy integrated number densities for neutrinos (first and third row) and antineutrinos (second and fourth row) as functions of radius for $t_{\text{pb}} = 0.5$ (top panels) and 1 s (bottom panels). The dashed curves correspond to the classical steady state solution obtained in the absence of flavor conversion, while the solid curves represent the quasi-steady state configuration obtained including flavor conversion and extracted after 1.25×10^{-4} s of simulation time. After neutrino decoupling flavor equipartition is achieved and the number densities of the different flavors become identical to each other. The radius of neutrino decoupling is marked through vertical lines in each plot and is minimally affected by flavor conversion. *Right:* Angle-integrated spectral energy distributions as functions of the neutrino energy, extracted at r_{max} for the classical steady state solution (dashed curves) and the quasi-steady state one (solid curves). Because of flavor conversion, the spectral energy distribution of ν_e ($\bar{\nu}_e$) almost coincides with the one of ν_x ($\bar{\nu}_x$) for both post-bounce times.

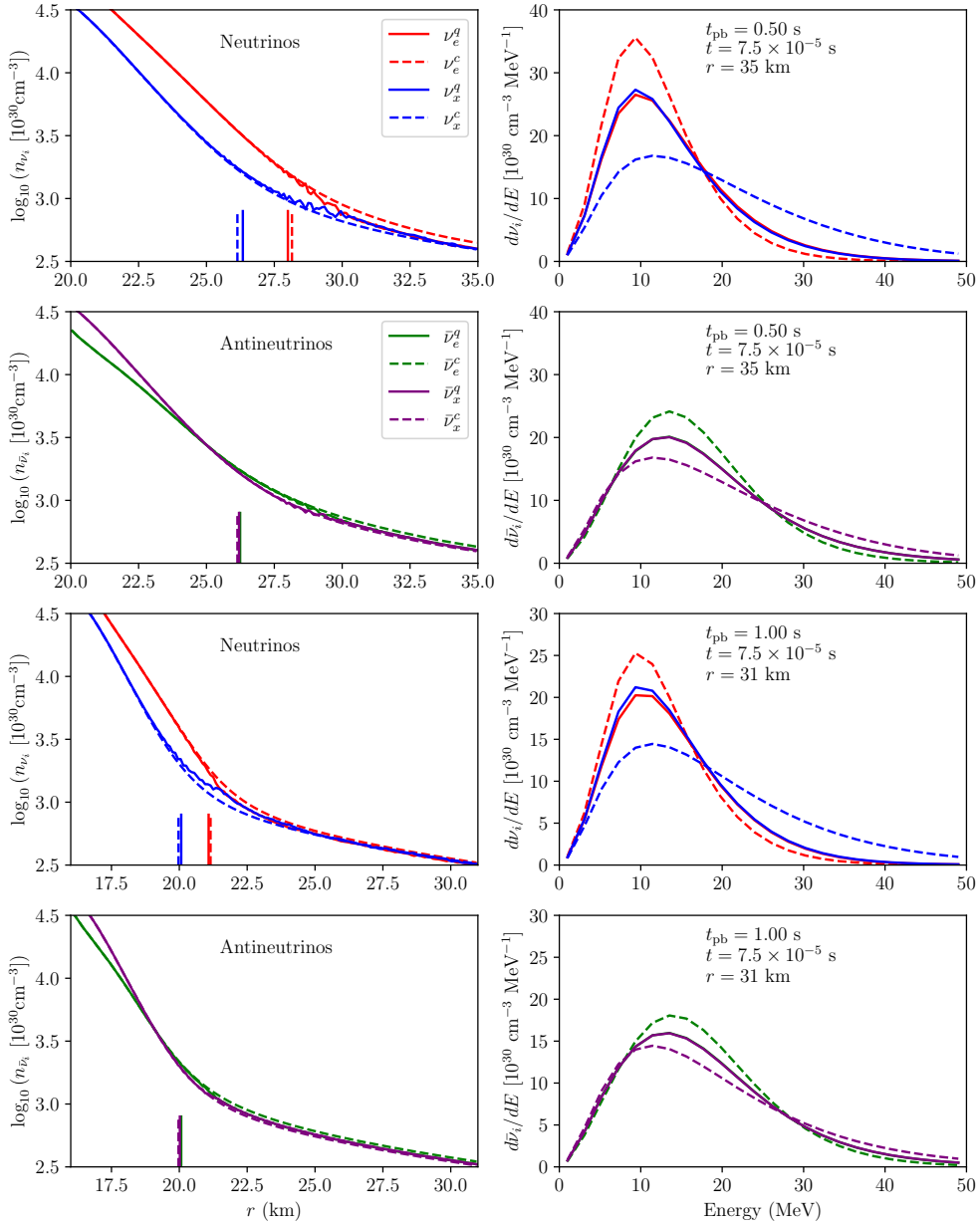


Figure 9. *Left:* Angle and energy integrated number densities for neutrinos (first and third row) and antineutrinos (second and fourth row) as functions of radius for $t_{\text{pb}} = 0.5$ (top panels) and 1 s (bottom panels). The dashed curves correspond to the classical steady state solution obtained in the absence of flavor conversion, while the solid curves represent the quasi-steady state configuration obtained including flavor conversion and extracted after 7.5×10^{-5} s of simulation time. After neutrino decoupling flavor equipartition is achieved and the number densities of the different flavors become identical to each other. The radius of neutrino decoupling is marked through vertical lines in each plot and is minimally affected by flavor conversion. *Right:* Angle-integrated spectral energy distributions as functions of the neutrino energy, extracted at r_{max} for the classical steady state solution (dashed curves) and the quasi-steady state one (solid curves). Because of flavor conversion, the spectral energy distribution of ν_e ($\bar{\nu}_e$) almost coincides with the one of ν_x ($\bar{\nu}_x$) for both post-bounce times.

as

$$\dot{\epsilon} = \dot{\epsilon}_{\nu_e} + \dot{\epsilon}_{\bar{\nu}_e} \quad \text{where,} \quad (5.1)$$

$$\begin{aligned} \dot{\epsilon}_{\nu_e} &= \sigma_0 \left(\frac{1 + 3g_A}{4} \right) \int_0^\infty dE \left(\frac{E + Q}{m_e c^2} \right)^2 \sqrt{(E + Q)^2 - m_e^2} \\ &\times \left[1 - \left(\frac{m_e c^2}{E + Q} \right) \right]^{\frac{1}{2}} \left(1 - 1.01 \frac{E}{m_n} \right) (1 - f_{e^-}) \frac{dn_{\nu_e}}{dE} \end{aligned} \quad (5.2)$$

$$\begin{aligned} \dot{\epsilon}_{\bar{\nu}_e} &= \sigma_0 \left(\frac{1 + 3g_A}{4} \right) \int_{m_e + Q}^\infty dE \left(\frac{E - Q}{m_e c^2} \right)^2 \sqrt{(E - Q)^2 - m_e^2} \\ &\times \left[1 - \left(\frac{m_e c^2}{E - Q} \right) \right]^{\frac{1}{2}} \left(1 - 7.1 \frac{E}{m_p} \right) \frac{dn_{\bar{\nu}_e}}{dE}, \end{aligned} \quad (5.3)$$

where E denotes the energy of ν_e or $\bar{\nu}_e$, $Q = 1.2933$ MeV denotes the Q -value of the β -reaction, $m_e = 0.511$ MeV is the mass of the electron, σ_0 is the characteristic neutrino interaction cross section ($4G_F^2 m_e^2 / \pi \approx 1.7 \times 10^{-44}$ cm²), $(1 - f_{e^-})$ is the electron Pauli-blocking factor, and $g_A = 1.27$ is the axial coupling.

Figure 12 shows that, for all cases except $t_{\text{pb}} = 0.12$ s (for which we do not see any flavor conversion), an increase in the heating rate by 15–25% occurs. This is not surprising since the flavor evolution increases the number density of electron type neutrinos in the high energy tail of the spectral distribution, and a larger heating rate is expected for larger neutrino energy. While we do not compute the neutrino cooling rate and do not take into account the feedback that the neutrino flavor conversion physics could have on the supernova hydrodynamic background, our results suggest a non-trivial impact of neutrino flavor conversion physics on the supernova mechanism, supporting earlier parametric studies [30–32].

Our findings should be considered with caution as they have been obtained relying on a spherically symmetric core-collapse supernova model. While we observe a non-trivial appearance of ELN crossings as a function of the post-bounce time in the classical solution of the Boltzmann equations, multi-dimensional core-collapse supernova simulations show evidence

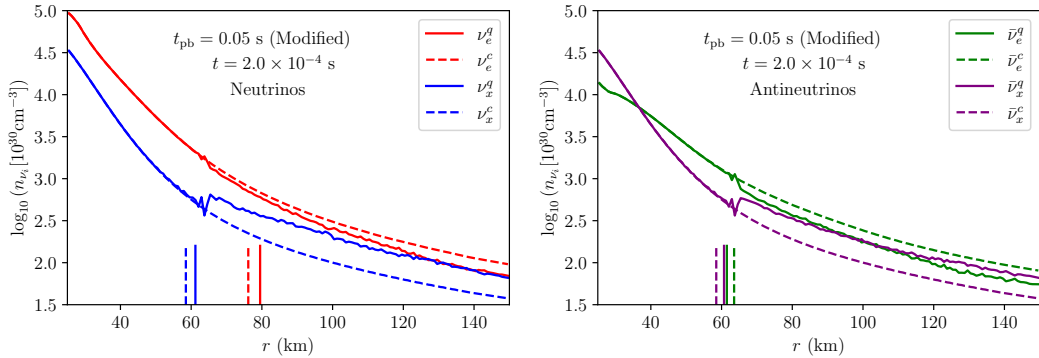


Figure 10. *Left:* Angle and energy integrated neutrino number densities for each flavor as functions of radius for the modified configuration obtained by changing the emission term of $\bar{\nu}_e$ by 20% at $t_{\text{pb}} = 0.05$ s. The quasi-steady state is extracted at $t = 2 \times 10^{-4}$ s (simulation time), starting from the classical steady state solution. It can be seen that ν_e does not reach equipartition with ν_x . *Right:* The same as the left panel, but for antineutrinos.

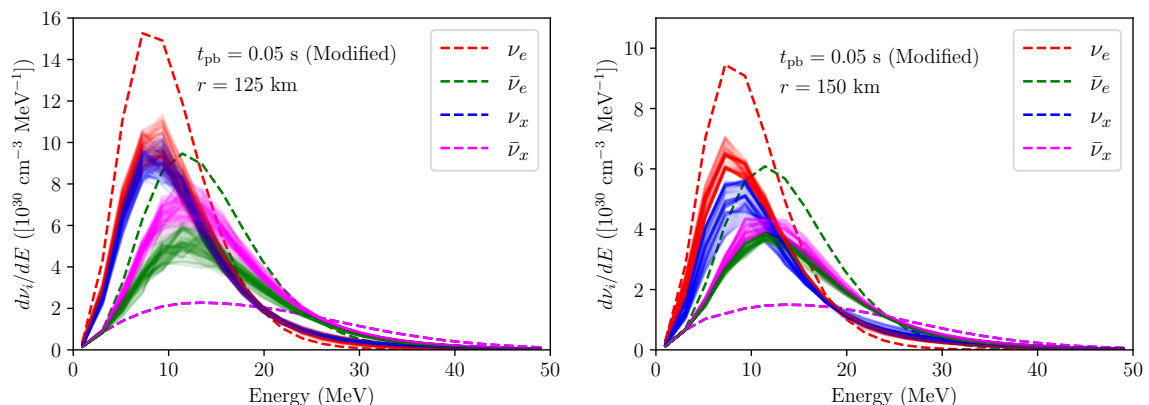


Figure 11. *Left:* Angle-integrated spectral energy distributions plotted for 200 selected simulation time steps between 1×10^{-4} and 2×10^{-4} s, and extracted at $r = 125$ km for the modified configuration obtained by increasing by 20% the emission term of $\bar{\nu}_e$ at $t_{\text{pb}} = 0.05$ s. The energy spectra fluctuate in time by almost 10%, with the ν_e spectrum going approximately in equipartition with ν_x . However, equipartition in the antineutrino sector is not achieved. *Right:* Same as the left panel, but for $r = 150$ km. A comparable variation of 10% in the energy distributions is observed in time once the quasi-steady state configuration is reached. In this case, the antineutrinos approach equipartition, but this is not the case for neutrinos.

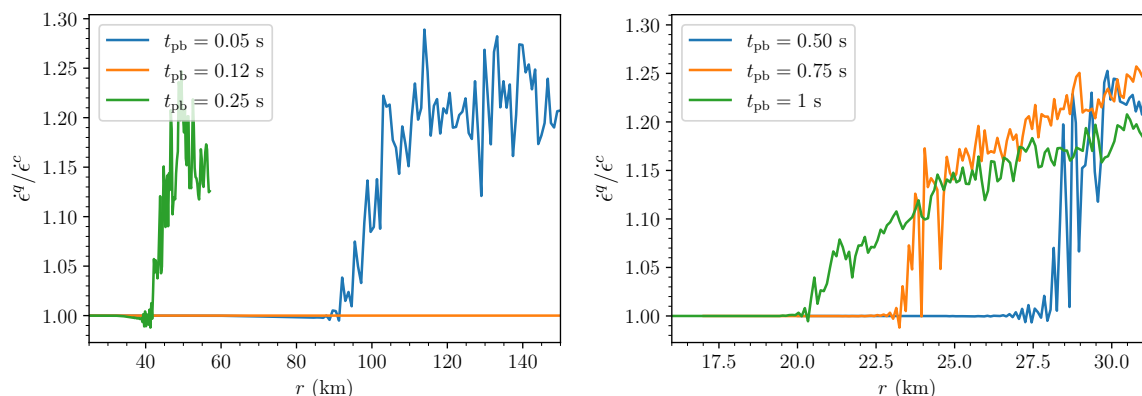


Figure 12. *Left:* Ratio between the neutrino heating rates obtained adopting the quasi-steady state angle-integrated neutrino distributions after solving the QKEs and the ones computed from the classical solution (i.e., neglecting flavor conversion) for early times, $t_{\text{pb}} = 0.05, 0.12$ and 0.25 s. At radii larger than the one of neutrino decoupling, the heating rate is increased by 15–25%, except for the case of $t_{\text{pb}} = 0.12$ s. *Right:* Same as the left panel but for late accretion times, $t_{\text{pb}} = 0.5, 0.75$ and 1 s.

of large scale asymmetries in the neutrino emission (e.g. due to the LESA instability [69]) and the location of flavor instabilities may be impacted [70].

In order to facilitate the numerical solution of the QKEs, we choose to attenuate the self-interaction strength by a constant factor 10^{-3} (see Eq. 2.6), nevertheless for all pot-bounce times we have that $\mu \gg \omega$ at neutrino decoupling. When flavor equipartition is reached, it is unlikely that the rescaling of the self-interaction strength can affect the results. However, for the earlier accretion phase ($t_{\text{pb}} \lesssim 0.5$ s), flavor equipartition is not reached, and it is possible that this scaling might slightly affect the exact final flavor outcome and the time needed to

reach a quasi-steady state solution.

The energy-dependent solution of the QKEs has consequences on the development of ELN crossings (cf. the corresponding single-energy solution presented in Ref. [23]) and therefore the presence of flavor instabilities; yet, for all post-bounce times, we find that a quasi-steady state configuration is achieved—cf. also Refs. [51, 71]. These findings support recent attempts aiming at forecasting the quasi-steady state flavor configuration due to flavor conversion or designing methods to incorporate such physics into neutrino-radiation-hydrodynamic simulations [35, 36, 41, 42, 72–74]; on the other hand, caution should be adopted in the forecast of the quasi-steady state neutrino configuration because of the dependence of the latter on the boundary conditions of the simulation box and features of the ELN distribution [34, 37, 41].

We find that flavor equipartition is obtained for $t_{\text{pb}} \gtrsim 0.5$ s. Such results may seem to confirm recent work in this direction [36, 39–49]. However, as shown through the flavor configuration obtained by tweaking the collision term in Sec. 4.3, we stress that flavor equipartition depends on the initial conditions and should not be considered a general outcome of global flavor simulations [33, 34, 37].

Similar to Ref. [22], we explore the flavor conversion physics for a range of neutrino flavor configurations linked to different post-bounce times. While our results are in general agreement with the ones of Ref. [22], we scan a broader range of post-bounce times highlighting time-dependent features of the flavor outcome. Moreover, differently from Ref. [22], we do not artificially tweak the electron abundance to favor the appearance of ELN crossings; this has implications on the relative relevance between collisional and fast flavor instabilities. We also confirm the preliminary findings of Refs. [22, 23, 70], where it was concluded that collisional instabilities do not affect the flavor composition significantly.

6 Conclusions

Understanding the neutrino flavor distribution resulting from flavor conversion occurring in the dense core of a supernova is crucial in order to investigate the impact of this physics on the supernova explosion mechanism. We numerically solve the neutrino quantum kinetic equations (QKEs) in a multi-energy and multi-angle framework and within a spherically symmetric shell, tracking neutrino decoupling.

We solve the QKEs adopting as inputs static hydrodynamic backgrounds extracted from a one-dimensional core-collapse supernova simulation with a mass of $18.6 M_{\odot}$ at post-bounce times $t_{\text{pb}} = 0.05, 0.12, 0.25, 0.5, 0.75,$ and 1 s. First, neglecting flavor conversion, we compute the angular distributions of neutrinos and antineutrinos, following Ref. [23]. Differently from Ref. [23] and because of the multi-energy numerical solution of the QKEs, we find that crossings in the electron neutrino lepton number (ELN) angular distributions appear for $t_{\text{pb}} \gtrsim 0.5$ s, but not at earlier post-bounce times.

We adopt the classical steady-state solution to solve the QKEs, this time taking into account neutrino flavor conversion. Fast flavor conversion is responsible for making the spectral energy distribution of ν_e ($\bar{\nu}_e$) equal to the one of ν_x ($\bar{\nu}_x$) for $t_{\text{pb}} \gtrsim 0.5$ s, i.e. flavor equipartition is reached. Despite the changes in the neutrino energy and angular distributions of all flavors, we find that the flavor-dependent neutrino decoupling radii are negligibly affected for the investigated flavor configurations; this is because of the relatively similar properties between the electron and the non-electron flavors characterizing the late accretion phase that facilitate flavor equipartition, but overall negligibly affect the energy and angle

integrated flavor-dependent number density at decoupling. On the other hand, ELN crossings are not found for $t_{\text{pb}} \lesssim 0.5$ s, but flavor conversion develops because of vacuum mixing, which effectively induces a crossing in the ELN angular distributions.

Remarkably, flavor equipartition is not a generic outcome of fast flavor conversion, but rather the result of the interplay between collisions, flavor conversion and advection, when the neutrino emission properties of the electron and non-electron flavors are reasonably comparable to each other. Modifying the collision term artificially for a time snapshot extracted at $t_{\text{pb}} \lesssim 0.5$ s to induce a crossing in the ELN angular distribution, we find that flavor equipartition is not achieved. This is because the differences in the emission properties of different flavors are larger in the early accretion phase and the interplay between flavor conversion and collisions cannot equilibrate the electron and non-electron flavors.

Our findings should be expanded to draw conclusions on the flavor conversion phenomenology expected in a broader range of core-collapse supernova models. Moreover, a self-consistent implementation of flavor conversion in supernova hydrodynamic simulations may dynamically change the neutrino emission properties as a function of the post-bounce time, in turn possibly affecting the flavor conversion phenomenology. Despite its intrinsic limitations, our work highlights a very interesting, non-trivial flavor phenomenology in core-collapse supernovae, calling for further investigation in order to assess its impact on the neutrino-driven explosion mechanism and nucleosynthesis.

Acknowledgments

This project has received support from the Danmarks Frie Forskningsfond (Project No. 8049-00038B), the European Union (ERC, ANET, Project No. 101087058), and the Deutsche Forschungsgemeinschaft through Sonderforschungsbereich SFB 1258 “Neutrinos and Dark Matter in Astro- and Particle Physics” (NDM). Views and opinions expressed are those of the authors only and do not necessarily reflect those of the European Union or the European Research Council. Neither the European Union nor the granting authority can be held responsible for them.

References

- [1] J. T. Pantaleone, *Neutrino flavor evolution near a supernova’s core*, *Phys. Lett. B* **342** (1995) 250–256, [[astro-ph/9405008](#)].
- [2] P. Langacker and J. Liu, *Standard Model contributions to the neutrino index of refraction in the early universe*, *Phys. Rev. D* **46** (1992) 4140–4160, [[hep-ph/9206209](#)].
- [3] A. Mirizzi, I. Tamborra, H.-T. Janka, N. Saviano, K. Scholberg, R. Bollig et al., *Supernova Neutrinos: Production, Oscillations and Detection*, *Riv. Nuovo Cim.* **39** (2016) 1–112, [[1508.00785](#)].
- [4] H. Duan, G. M. Fuller and Y.-Z. Qian, *Collective Neutrino Oscillations*, *Ann. Rev. Nucl. Part. Sci.* **60** (2010) 569–594, [[1001.2799](#)].
- [5] S. Chakraborty, R. Hansen, I. Izaguirre and G. G. Raffelt, *Collective neutrino flavor conversion: Recent developments*, *Nucl. Phys. B* **908** (2016) 366–381, [[1602.02766](#)].
- [6] I. Tamborra and S. Shalgar, *New Developments in Flavor Evolution of a Dense Neutrino Gas*, *Ann. Rev. Nucl. Part. Sci.* **71** (2021) 165–188, [[2011.01948](#)].
- [7] S. Richers and M. Sen, *Fast Flavor Transformations*, pp. 1–17. Springer Nature Singapore, Singapore, 2022. [[2207.03561](#)]. 10.1007/978-981-15-8818-1_125-1.

- [8] H. Duan, G. M. Fuller and Y.-Z. Qian, *Collective neutrino flavor transformation in supernovae*, *Phys. Rev. D* **74** (2006) 123004, [[astro-ph/0511275](#)].
- [9] H. Duan, G. M. Fuller, J. Carlson and Y.-Z. Qian, *Simulation of Coherent Non-Linear Neutrino Flavor Transformation in the Supernova Environment. 1. Correlated Neutrino Trajectories*, *Phys. Rev. D* **74** (2006) 105014, [[astro-ph/0606616](#)].
- [10] R. F. Sawyer, *Speed-up of neutrino transformations in a supernova environment*, *Phys. Rev. D* **72** (2005) 045003, [[hep-ph/0503013](#)].
- [11] R. F. Sawyer, *The multi-angle instability in dense neutrino systems*, *Phys. Rev. D* **79** (2009) 105003, [[0803.4319](#)].
- [12] R. F. Sawyer, *Neutrino cloud instabilities just above the neutrino sphere of a supernova*, *Phys. Rev. Lett.* **116** (2016) 081101, [[1509.03323](#)].
- [13] S. Chakraborty, R. S. Hansen, I. Izaguirre and G. G. Raffelt, *Self-induced neutrino flavor conversion without flavor mixing*, *JCAP* **03** (2016) 042, [[1602.00698](#)].
- [14] I. Izaguirre, G. G. Raffelt and I. Tamborra, *Fast Pairwise Conversion of Supernova Neutrinos: A Dispersion-Relation Approach*, *Phys. Rev. Lett.* **118** (2017) 021101, [[1610.01612](#)].
- [15] L. Johns, *Collisional Flavor Instabilities of Supernova Neutrinos*, *Phys. Rev. Lett.* **130** (2023) 191001, [[2104.11369](#)].
- [16] T. Morinaga, *Fast neutrino flavor instability and neutrino flavor lepton number crossings*, *Phys. Rev. D* **105** (2022) L101301, [[2103.15267](#)].
- [17] S. Hannestad, G. G. Raffelt, G. Sigl and Y. Y. Y. Wong, *Self-induced conversion in dense neutrino gases: Pendulum in flavour space*, *Phys. Rev. D* **74** (2006) 105010, [[astro-ph/0608695](#)].
- [18] L. Johns and Z. Xiong, *Collisional instabilities of neutrinos and their interplay with fast flavor conversion in compact objects*, *Phys. Rev. D* **106** (2022) 103029, [[2208.11059](#)].
- [19] I. Padilla-Gay, I. Tamborra and G. G. Raffelt, *Neutrino fast flavor pendulum. II. Collisional damping*, *Phys. Rev. D* **106** (2022) 103031, [[2209.11235](#)].
- [20] Y.-C. Lin and H. Duan, *Collision-induced flavor instability in dense neutrino gases with energy-dependent scattering*, *Phys. Rev. D* **107** (2023) 083034, [[2210.09218](#)].
- [21] Z. Xiong, M.-R. Wu, G. Martínez-Pinedo, T. Fischer, M. George, C.-Y. Lin et al., *Evolution of collisional neutrino flavor instabilities in spherically symmetric supernova models*, *Phys. Rev. D* **107** (2023) 083016, [[2210.08254](#)].
- [22] H. Nagakura and M. Zaizen, *Basic characteristics of neutrino flavor conversions in the postshock regions of core-collapse supernova*, *Phys. Rev. D* **108** (2023) 123003, [[2308.14800](#)].
- [23] S. Shalgar and I. Tamborra, *Do neutrinos become flavor unstable due to collisions with matter in the supernova decoupling region?*, *Phys. Rev. D* **109** (2024) 103011, [[2307.10366](#)].
- [24] S. A. Colgate and R. H. White, *The Hydrodynamic Behavior of Supernovae Explosions*, *Astrophys. J.* **143** (1966) 626.
- [25] H. A. Bethe and J. R. Wilson, *Revival of a stalled supernova shock by neutrino heating*, *Astrophys. J.* **295** (1985) 14–23.
- [26] H. T. Janka, T. Melson and A. Summa, *Physics of Core-Collapse Supernovae in Three Dimensions: a Sneak Preview*, *Ann. Rev. Nucl. Part. Sci.* **66** (2016) 341–375, [[1602.05576](#)].
- [27] B. Müller, *Hydrodynamics of core-collapse supernovae and their progenitors*, *Astrophysics* **6** (2020) 3, [[2006.05083](#)].

- [28] A. Mezzacappa, E. Endeve, O. E. Bronson Messer and S. W. Bruenn, *Physical, numerical, and computational challenges of modeling neutrino transport in core-collapse supernovae*, *Liv. Rev. Comput. Astrophys.* **6** (2020) 4, [2010.09013].
- [29] A. Burrows and D. Vartanyan, *Core-Collapse Supernova Explosion Theory*, *Nature* **589** (2021) 29–39, [2009.14157].
- [30] J. Ehring, S. Abbar, H.-T. Janka, G. G. Raffelt and I. Tamborra, *Fast neutrino flavor conversion in core-collapse supernovae: A parametric study in 1D models*, *Phys. Rev. D* **107** (2023) 103034, [2301.11938].
- [31] J. Ehring, S. Abbar, H.-T. Janka, G. G. Raffelt and I. Tamborra, *Fast Neutrino Flavor Conversions Can Help and Hinder Neutrino-Driven Explosions*, *Phys. Rev. Lett.* **131** (2023) 061401, [2305.11207].
- [32] H. Nagakura, *Roles of Fast Neutrino-Flavor Conversion on the Neutrino-Heating Mechanism of Core-Collapse Supernova*, *Phys. Rev. Lett.* **130** (2023) 211401, [2301.10785].
- [33] S. Shalgar and I. Tamborra, *Neutrino decoupling is altered by flavor conversion*, *Phys. Rev. D* **108** (2023) 043006, [2206.00676].
- [34] S. Shalgar and I. Tamborra, *Neutrino flavor conversion, advection, and collisions: Toward the full solution*, *Phys. Rev. D* **107** (2023) 063025, [2207.04058].
- [35] H. Nagakura and M. Zaizen, *Connecting small-scale to large-scale structures of fast neutrino-flavor conversion*, *Phys. Rev. D* **107** (2023) 063033, [2211.01398].
- [36] Z. Xiong, M.-R. Wu, M. George and C.-Y. Lin, *Robust integration of fast flavor conversions in classical neutrino transport*, **2403.17269**.
- [37] M. Cornelius, S. Shalgar and I. Tamborra, *Perturbing fast neutrino flavor conversion*, *JCAP* **02** (2024) 038, [2312.03839].
- [38] S. Shalgar, I. Padilla-Gay and I. Tamborra, *Neutrino propagation hinders fast pairwise flavor conversions*, *JCAP* **06** (2020) 048, [1911.09110].
- [39] Z. Xiong, M.-R. Wu, M. George, C.-Y. Lin, N. K. Largani, T. Fischer et al., *Fast neutrino flavor conversions in a supernova: emergence, evolution, and effects*, **2402.19252**.
- [40] J. D. Martin, J. Carlson, V. Cirigliano and H. Duan, *Fast flavor oscillations in dense neutrino media with collisions*, *Phys. Rev. D* **103** (2021) 063001, [2101.01278].
- [41] M. Zaizen and H. Nagakura, *Characterizing quasisteady states of fast neutrino-flavor conversion by stability and conservation laws*, *Phys. Rev. D* **107** (2023) 123021, [2304.05044].
- [42] M. Zaizen and H. Nagakura, *Simple method for determining asymptotic states of fast neutrino-flavor conversion*, *Phys. Rev. D* **107** (2023) 103022, [2211.09343].
- [43] Z. Xiong, M.-R. Wu, S. Abbar, S. Bhattacharyya, M. George and C.-Y. Lin, *Evaluating approximate asymptotic distributions for fast neutrino flavor conversions in a periodic 1D box*, *Phys. Rev. D* **108** (2023) 063003, [2307.11129].
- [44] E. Grohs, S. Richers, S. M. Couch, F. Foucart, J. P. Kneller and G. C. McLaughlin, *Neutrino fast flavor instability in three dimensions for a neutron star merger*, *Phys. Lett. B* **846** (2023) 138210, [2207.02214].
- [45] S. Richers, D. Willcox and N. Ford, *Neutrino fast flavor instability in three dimensions*, *Phys. Rev. D* **104** (2021) 103023, [2109.08631].
- [46] S. Richers, H. Duan, M.-R. Wu, S. Bhattacharyya, M. Zaizen, M. George et al., *Code comparison for fast flavor instability simulations*, *Phys. Rev. D* **106** (2022) 043011, [2205.06282].
- [47] S. Bhattacharyya and B. Dasgupta, *Fast Flavor Depolarization of Supernova Neutrinos*, *Phys. Rev. Lett.* **126** (2021) 061302, [2009.03337].

- [48] S. Bhattacharyya and B. Dasgupta, *Elaborating the ultimate fate of fast collective neutrino flavor oscillations*, *Phys. Rev. D* **106** (2022) 103039, [2205.05129].
- [49] M.-R. Wu, M. George, C.-Y. Lin and Z. Xiong, *Collective fast neutrino flavor conversions in a 1D box: Initial conditions and long-term evolution*, *Phys. Rev. D* **104** (2021) 103003, [2108.09886].
- [50] “Garching core-collapse supernova data archive.”
<https://wwwmpa.mpa-garching.mpg.de/ccsnarchive/data/Bollig2016/>.
- [51] H. Nagakura and M. Zaizen, *Time-Dependent and Quasisteady Features of Fast Neutrino-Flavor Conversion*, *Phys. Rev. Lett.* **129** (2022) 261101, [2206.04097].
- [52] S. Shalgar, I. Tamborra and M. Bustamante, *Core-collapse supernovae stymie secret neutrino interactions*, *Phys. Rev. D* **103** (2021) 123008, [1912.09115].
- [53] I. Padilla-Gay, S. Shalgar and I. Tamborra, *Multi-Dimensional Solution of Fast Neutrino Conversions in Binary Neutron Star Merger Remnants*, *JCAP* **01** (2021) 017, [2009.01843].
- [54] A. Burrows, S. Reddy and T. A. Thompson, *Neutrino opacities in nuclear matter*, *Nucl. Phys. A* **777** (2006) 356–394, [astro-ph/0404432].
- [55] H.-T. Janka, *Explosion Mechanisms of Core-Collapse Supernovae*, *Ann. Rev. Nucl. Part. Sci.* **62** (2012) 407–451, [1206.2503].
- [56] T. A. Thompson, *Topics in the theory of core-collapse supernovae*, Ph.D. thesis, The University of Arizona., 2002.
- [57] E. O’Connor, *An Open-Source Neutrino Radiation Hydrodynamics Code for Core-Collapse Supernovae*, *Astrophys. J. Suppl.* **219** (2015) 24, [1411.7058].
- [58] A. Weiss, W. Hillebrandt, H. C. Thomas and H. Ritter, *Cox and Giuli’s Principles of Stellar Structure*. Cambridge Scientific Publishers LTD, Cambridge, UK, 2006.
- [59] T. Morinaga and S. Yamada, *Linear stability analysis of collective neutrino oscillations without spurious modes*, *Phys. Rev. D* **97** (2018) 023024, [1803.05913].
- [60] A. Esteban-Pretel, A. Mirizzi, S. Pastor, R. Tomàs, G. G. Raffelt, P. D. Serpico et al., *Role of dense matter in collective supernova neutrino transformations*, *Phys. Rev. D* **78** (2008) 085012, [0807.0659].
- [61] S. Sarikas, I. Tamborra, G. G. Raffelt, L. Huedepohl and H.-T. Janka, *Supernova neutrino halo and the suppression of self-induced flavor conversion*, *Phys. Rev. D* **85** (2012) 113007, [1204.0971].
- [62] N. Saviano, S. Chakraborty, T. Fischer and A. Mirizzi, *Stability analysis of collective neutrino oscillations in the supernova accretion phase with realistic energy and angle distributions*, *Phys. Rev. D* **85** (2012) 113002, [1203.1484].
- [63] S. Chakraborty, T. Fischer, A. Mirizzi, N. Saviano and R. Tomàs, *No collective neutrino flavor conversions during the supernova accretion phase*, *Phys. Rev. Lett.* **107** (2011) 151101, [1104.4031].
- [64] S. Chakraborty, T. Fischer, A. Mirizzi, N. Saviano and R. Tomàs, *Analysis of matter suppression in collective neutrino oscillations during the supernova accretion phase*, *Phys. Rev. D* **84** (2011) 025002, [1105.1130].
- [65] S. Chakraborty, G. Raffelt, H.-T. Janka and B. Müller, *Supernova deleptonization asymmetry: Impact on self-induced flavor conversion*, *Phys. Rev. D* **92** (2015) 105002, [1412.0670].
- [66] P. Dedin Neto, I. Tamborra and S. Shalgar, *Fast Conversion of Neutrinos: Energy Dependence of Flavor Instabilities*, 2312.06556.
- [67] I. Tamborra, L. Huedepohl, G. Raffelt and H.-T. Janka, *Flavor-dependent neutrino angular distribution in core-collapse supernovae*, *Astrophys. J.* **839** (2017) 132, [1702.00060].

- [68] M.-R. Wu, I. Tamborra, O. Just and H.-T. Janka, *Imprints of neutrino-pair flavor conversions on nucleosynthesis in ejecta from neutron-star merger remnants*, *Phys. Rev. D* **96** (2017) 123015, [[1711.00477](#)].
- [69] I. Tamborra, F. Hanke, H.-T. Janka, B. Müller, G. G. Raffelt and A. Marek, *Self-sustained asymmetry of lepton-number emission: A new phenomenon during the supernova shock-accretion phase in three dimensions*, *Astrophys. J.* **792** (2014) 96, [[1402.5418](#)].
- [70] R. Akaho, J. Liu, H. Nagakura, M. Zaizen and S. Yamada, *Collisional and fast neutrino flavor instabilities in two-dimensional core-collapse supernova simulation with Boltzmann neutrino transport*, *Phys. Rev. D* **109** (2024) 023012, [[2311.11272](#)].
- [71] C. Kato, H. Nagakura and M. Zaizen, *Flavor conversions with energy-dependent neutrino emission and absorption*, *Phys. Rev. D* **108** (2023) 023006, [[2303.16453](#)].
- [72] S. Abbar, M.-R. Wu and Z. Xiong, *Application of neural networks for the reconstruction of supernova neutrino energy spectra following fast neutrino flavor conversions*, *Phys. Rev. D* **109** (2024) 083019, [[2401.17424](#)].
- [73] H. Nagakura, L. Johns and M. Zaizen, *Bhatnagar-Gross-Krook subgrid model for neutrino quantum kinetics*, *Phys. Rev. D* **109** (2024) 083013, [[2312.16285](#)].
- [74] S. Abbar, M.-R. Wu and Z. Xiong, *Physics-informed neural networks for predicting the asymptotic outcome of fast neutrino flavor conversions*, *Phys. Rev. D* **109** (2024) 043024, [[2311.15656](#)].